Enhancement of Topical Delivery from Biodegradable Nanoparticles

Rocío Alvarez-Román,[1,2,3] Aarti Naik,[1,3] Yogeshvar N. Kalia,[1,3] Richard H. Guy,[1,3,4] and Hatem Fessi[1,2]

Received March 24, 2004; accepted June 29, 2004

Purpose. To determine whether and how encapsulation of lipophilic compounds in polymeric nanoparticles is able to improve topical delivery to the skin.

Methods. The penetration of octyl methoxycinnamate (OMC; Parsol MCX), a highly lipophilic sunscreen, into and across porcine ear skin *in vitro* was investigated, subsequent to encapsulation in poly(ε-caprolactone) nanoparticles, using tape-stripping. Confocal laser scanning microscopy (CLSM) was used to visualize the distribution of nanoparticles, charged with Nile red (NR), a lipophilic and fluorescent dye.

Results. Quantification of OMC in the skin using tape-stripping demonstrated that nanoparticulate encapsulation produced a 3.4-fold increase in the level of OMC within the stratum corneum (SC), although the use of nanoparticles did not appear to increase skin permeation (it was not possible to detect OMC in the receiver compartment after 6 h). The confocal images showed that the fluorescence profile observed in the skin after application of NR-containing nanoparticles was clearly different from that seen following application of NR dissolved in propylene glycol. Two hours post-application of NR-containing nanoparticles, fluorescence was perceptible at greater depths (up to 60 μm) within the skin.

Conclusions. i) Nanoparticulate encapsulation of OMC increased its "availability" with the SC. ii) The altered distribution of NR when delivered via nanoparticles was due, at least in part, to its altered thermodynamic activity (relative to that in propylene glycol) and, as a result, an increase in its partition coefficient into the SC.

KEY WORDS: CLSM; fluorescence; nanoparticles; skin; tape stripping.

INTRODUCTION

The composition and excellent barrier function of the skin limits the number of suitable drugs for transdermal delivery to small, moderately lipophilic, and highly potent molecules. Although moderate lipophilicity (log $K_{o/w}$ ~2) is frequently advantageous for partitioning of the drug from a formulation into the skin, highly lipophilic molecules do not transfer well from the lipidic stratum corneum into the more aqueous viable epidermis and, as a result, are often poorly permeable. Although strategies for improving cutaneous delivery, including complex physical enhancement methods, for example, iontophoresis, sonophoresis, and electroporation, have been developed, these techniques are more suited to hydrophilic, water-soluble substances. With respect to passive enhancement methods, supersaturated formulations or novel vehicle systems, for example, microemulsions, liposomes, and colloidal polymeric suspensions, have also been investigated as alternatives to the more "classic" chemical penetration enhancer systems. Nevertheless, the percutaneous penetration of highly lipophilic molecules remains problematic.

Drug encapsulation, through judicious choice of the polymeric material, is a useful pharmaceutical strategy for modifying the physicochemical properties of the encapsulated molecule and offers a means to facilitate the percutaneous delivery of difficult-to-uptake substances. A limited number of biodegradable, polymer microparticles (1,2) and solid-lipid nanoparticles (SLN) (3–6) have been investigated with respect to their potential for transdermal drug administration, for example, for adapalene, acyclovir, and vitamins A and E. The use of PLGA-microparticles as vehicles for topical drug delivery, providing a reservoir system for release into the skin, has also been studied (7). However, a more fundamental understanding of i) the mechanism(s) of interaction between these novel drug delivery systems and the skin, and ii) the transport pathways within the membrane, is required to establish the feasibility of using such polymeric nanoparticles to optimize the transport process.

Confocal laser scanning microscopy offers the possibility of visualizing the distribution of a fluorescent probe in the sample by optical sectioning without cryofixation or embedding the tissue. Hence, this non-intrusive technique is a valuable method for reporting on the extent of penetration of molecules into the skin and for identifying transport pathways as evidenced by hotspots of fluorescence intensity.

The objective of this study was to investigate the passive skin penetration and permeation of highly lipophilic substrates encapsulated within biodegradable poly(ε-caprolactone) nanoparticles, prepared by the solvent displacement procedure. In the first part of the study, standard permeation experiments and a tape-stripping technique were used to investigate the distribution of encapsulated OMC across excised porcine skin. In the second phase, confocal laser scanning microscopy was used to visualize the permeation of biodegradable poly(ε-caprolactone) nanoparticles containing Nile red, a lipophilic, fluorescent probe.

MATERIALS AND METHODS

Chemicals

The polymer poly(ε-caprolactone) P(CL), (MW: 10 000), was supplied by Fluka (Saint Quentin Fallavier, France). Octyl methoxycinnamate (Parsol MCX), OMC, was obtained from Givaudan-Roure (Vernier, Switzerland). Polysorbate 85, P-85, (Tween 85) was purchased from Atlas Chemie, Germany. Polysorbate 80, P-80 (Tween 80), Nile red (NR), propylene glycol (PG), and phosphate buffer were supplied by Sigma-Aldrich Chimie (Saint Quentin Fallavier, France). Ac-

[1] Centre interuniversitaire de recherche et d'enseignement, Universities of Geneva and Lyon, Archamps, France.
[2] UMR CNRS 5007, Claude Bernard University, Lyon, France.
[3] School of Pharmacy, University of Geneva, Geneva, Switzerland.
[4] To whom correspondence should be addressed. (e-mail: r.h.guy@bath.ac.uk)

ABBREVIATIONS: CLSM, confocal laser scanning microscopy; EM, emulsion; EtOH, ethanol; IPM, isopropyl myristate; NP, nanoparticles; NR, Nile red; NR-NP, fluorescent-NP; NR-PG, NR-solution in PG; NR-S, saturated solution of NR in PG; OMC, octyl methoxycinnamate; P-80, polysorbate 80; P-85, polysorbate 85; PB, phosphate buffer; P(CL), poly(ε-caprolactone); PG, propylene glycol; PLGA, poly(lactide-co-glycodide)acide; SC, stratum corneum; SLN, solid-lipid nanoparticles.

0724-8741/04/1000-1818/0 © 2004 Springer Science+Business Media, Inc.

etone, ethanol (EtOH), and isopropyl myristate (IPM) were purchased from Fluka (Saint Quentin Fallavier, France).

Preparation and Characterization of the Drug Carrier Systems

OMC-loaded P(CL) nanoparticles (NP) were prepared by the solvent displacement procedure previously described (8). An acetone solution containing 125 mg of P(CL) and 510 mg of OMC was injected into 50 ml of an aqueous solution containing 3% (w/v of the aqueous phase) of polysorbate 85. The aqueous phase immediately turned milky with bluish opalescence due to the formation of a nanoparticulate suspension (OMC-NP). The acetone was then removed under reduced pressure at 35–40°C for approximately 10 min. The OMC-NP suspension was concentrated to the desired final volume (10–20 ml) by removal of water under the same conditions. An OMC-emulsion (OMC-EM) was prepared by the same method as the nanoparticles, omitting the polymer. Fluorescent-nanoparticles (NR-NP) were prepared using the same procedure as for the OMC-NP, replacing OMC with 0.02% (w/w) of NR in the organic phase. Two fluorescent control solutions were used: a NR-solution in PG (NR-PG) at the same NR concentration as in the nanoparticles and a saturated solution of NR in PG (NR-S).

The mean size and polydispersity (index from 0 to 9) of the nanoparticle formulations were measured with a Coulter Nano-sizer (Coulter Electronics, Margency, France). A higher value indicates a less homogeneous nanoparticle size distribution. Measurements in monomodal distribution were made in triplicate for all prepared batches. Total OMC was determined after dissolution of NP in acetonitrile. The amount of un-encapsulated OMC was determined in the clear supernatant following separation of the NP from the aqueous medium by a combined ultrafiltration-centrifugation technique (Ultrafree-MC, Millipore, Bedford, MA, USA) (9). The equivalent acetonitrile volume was added in the supernatant. The OMC content in the NP was calculated by determining the difference between the total and free estimated drug concentrations. Measurements were made in quintuplicate by HPLC. Final concentration of OMC was 84 ± 5 μmol/ml and 83 ± 2 μmol/ml, respectively, for OMC-NP and OMC-EM. In the case of NR-NP, the measurements were made by spectrofluorimetry (Perkin-Elmer LS-3B, Rodgau-Jügesheim, Germany). The excitation and emission were performed at wavelengths of 543 nm and 630 nm, respectively. The detection limit was 2.1 pmol/ml. Final concentration of NR was 5 ± 0.8 nmol/ml for NR-NP.

The *in vitro* release behavior of NR from the NR-NP and NR-PG was also studied. A small vial (cross-sectional area = 1.13 cm^2) containing ~5.5 ml of either an aqueous suspension of NR-NP, or an equivalent volume of NR-PG was placed in a flask containing 200 ml of receptor medium (IPM). The system was thermostatted at 37 ± 2°C under constant stirring (200 rpm). The receptor medium was sampled at fixed time intervals and assayed for NR by spectrofluorimetry in order to establish the release rate of NR from the two formulations.

Skin Permeation Experiments

Full-thickness porcine ear skin was obtained from the slaughterhouse (S.O.D.E.X.A., Annecy, France). The subcutaneous fat was removed from the skin and the tissue was stored frozen for a maximum of two weeks before use. The skin was thawed and clamped into position between the donor and the receptor compartment of a vertical diffusion cell. The epidermal surface (area = 3.14 cm^2) was hydrated for 1 h with phosphate buffer (pH 7.4) and subsequently dried with a cotton swab. The donor compartment was then filled with 3 ml of the OMC carrier systems (80 μmol/ml of OMC encapsulated in NP or 83 μmol/ml of OMC in EM) and covered to prevent evaporation. The receptor medium consisting of phosphate buffer incorporating Tween 80 (5% v/v), was thermostatted at 37 ± 2°C under constant magnetic stirring. The solubility of the OMC in the receptor medium was determined prior to the experiments. The receptor medium was collected from the diffusion cell at 6 h and analyzed by HPLC. Experiments were performed in quintuplicate.

Tape Stripping

At the end of the permeation experiment, the excess formulation was removed from the skin surface. The skin was washed 3 times with phosphate buffer (pH 7.4) and dried gently with a cotton swab. Serial tape-stripping involving the removal of 15 strips using adhesive tape (polypropylene backing and acrylic adhesive; Scotch 845 Book Tape, 3M, St. Louis, MO, USA) was then conducted. Each tape was carefully weighed before and after the procedure with a 10 μg precision balance (Mettler AT 261, Greifensee, Switzerland). The OMC in the adhesive tapes was extracted, using a mixture of acetonitrile and water (85:15 v/v) and analyzed by HPLC. Validation of the extraction (in quintuplicate) was carried out using the same procedure, by spiking tape stripped samples of untreated SC with 250 μl of an OMC emulsion (350 nmol/ml). Validation of the OMC-NP extraction was performed with the same method. Compound recovery was 99 ± 1% and 86.4 ± 2%, respectively, for OMC-EM and OMC-NP in the HPLC analyses.

HPLC Analyses

All OMC samples from the permeation experiments (receptor medium and tapes) were quantified by HPLC analysis (Dionex, Sunnyvale, CA, USA) with UV detection at 310 nm, using a Hypersil BDS C8 (5 μm) 150 × 4.6 mm column (Supelco, Bellefonte, PA, USA). The mobile phase consisted of acetonitrile and water (85:15 v/v), acidified with orthophosphoric acid (pH 2.5), which was delivered at a flow-rate of 1 ml/min. The retention time for OMC was 4.1 min. The detection limit was 0.34 nmol/ml.

Solubility Determination of NR

Saturated solutions of NR were prepared by stirring an excess of the molecule in water, IPM or PG at room temperature (25 ± 1°C) for 24 h. The samples were centrifuged at 3000 rpm for 10 min, and the supernatants were subsequently filtered through a Nylon membrane (pore size 0.45 μm), then diluted with the respective vehicle and analyzed by spectrofluorimetry. Five replicate measurements in each solvent were made and revealed the following solubilities: water, 0.018 ± 0.003 μg/ml; PG, 174.7 ± 11.9 μg/ml; IPM, 340.6 ± 15.7 μg/ml.

Permeation Experiments Using NR-Carrier Systems

The skin was thawed and clamped into position between the donor and the receptor compartment of a vertical diffusion cell. The donor side of the skin (area = 3.14 cm^2) was hydrated for 1 h with phosphate buffer (pH 7.4) and subsequently dried with a cotton swab. The donor compartment was then filled with 3 ml of one of the NR-carrier systems: 6.3 nmol/ml of NR-NP, NR-PG, or NR-S. The receptor medium, consisting of PB and Tween 80 (5% v/v), was thermostatted at 37 ± 2°C under constant, magnetic stirring. The free or encapsulated NR formulations were placed in contact with the skin for 0.5, 1 and 2 h.

Confocal Laser Scanning Microscopy

At the end of the NR permeation experiments, the excess formulation was removed from the skin surface. The skin was then washed three times with phosphate buffer and dried gently with a cotton swab. The membranes were directly mounted, SC side up on a glass slide, and examined microscopically without additional tissue processing.

An LSM 410 Invert Laser Scan Microscope (Carl Zeiss, Göttingen, Germany) was used for imaging. The system is equipped with an argon-krypton laser (excitation lines at 488 and 568 nm). Confocal images were obtained using a Planneofluar 100×/0.30 oil immersion objective. The excitation and emission wavelengths were 543 nm and 630 nm, respectively. To determine the autofluorescence properties of the skin, samples were first investigated with the confocal microscope in the absence of the fluorescent probes. The autofluorescence of porcine skin was corrected at the confocal settings used in this study (data not shown). To visualize the distribution of NR fluorescence, confocal images were first obtained as *xy*-planes (i.e., parallel to the plane of the skin surface). The skin surface (z = 0 μm) is defined (by the user) as the imaging plane of brightest fluorescence with a morphology characteristic of the stratum corneum surface. To generate an *xz*-section, a horizontal line is "drawn" across a region of interest in the z = 0-μm *xy*-plane and is then "optically sliced" through the digitized image data of the successive *xy*-sections; the results are (*xz*-planar) optical cross-sections. All images were the average of four scans, and were obtained with the same optical aperture, lens and scan speed.

The images presented in the figures are necessarily representative and attempt to capture what was typically observed under each control and treatment condition. To assure an appropriate "representativeness," each image chosen was selected from a minimum of 90 and a maximum of 120 replicates.

RESULTS AND DISCUSSION

Table I shows the physical parameters of the nanoparticle formulation used in the *in vitro* permeation experiments. The results indicate that the solvent displacement method enabled the preparation of nanoparticles with high OMC loading efficiency (>90%), as expected from the high log $K_{oct/water}$ of the sunscreen (10). This result is consistent with other studies, in which similar, high loading efficiencies were obtained upon encapsulation of lipophilic drugs in NP, for example, >90% for indomethacin (11) and ~80% for primidone (12).

Table I. Physical Parameters of OMC-Nanoparticles (OMC-NP) Used in the Tape-Stripping Study and of Fluorescent-Nanoparticles (NR-NP) Used in Confocal Laser Scanning Microscopy

Formulation	Mean size ±SD[a] (nm)	PI[b] ± SD[a]	% encapsulated ±SD[a] (%)
OMC-NP	255 ± 5	2 ± 1	98 ± 1
NR-NP	250 ± 8	2 ± 1	80 ± 2

[a] SD, standard deviation (n = 3).
[b] PI, polydispersity index of the size distribution (expressed using a 0–9 scale).

In vitro passive permeation experiments involving a 6 h occlusive application of OMC-NP and OMC-EM revealed that the amount of OMC in the receptor compartment was below the limit of detection. Parenthetically, in the case of OMC, this result is quite propitious since OMC, a sunscreen agent, is intended to act on the surface of the skin and is required to permeate as little as possible into the deeper skin tissue in order to ensure its photoprotective function while avoiding systemic toxicity. Similar findings have been reported in the literature; for example, Potard *et al.* (10) showed that negligible amounts of OMC permeated across freshly dermatomed human skin and into the receptor fluid after a 16 h exposure. This absence of OMC permeation is likely due to its extremely high octanol-water partition coefficient (10). However, the absence of detectable permeation with OMC-nanoparticles in this study suggests, at first sight, that encapsulation does not facilitate transport into and across the porcine epidermis.

It is clear that skin penetration depends strongly on the physicochemical properties of the active compound and the vehicle in which it is applied; for example, particle size, type of vehicle (3). As mentioned above, this property is particularly important for sunscreens because it has been suggested that the amount of sunscreen inside the stratum corneum (SC) may be directly related to its sun protection factor value (13,14). In order to determine the OMC distribution in the skin, we used a stripping technique consisting of the progressive removal of SC with an adhesive tape (15). Figure 1 shows the total quantity of OMC recovered in the SC after 6 h of permeation from the emulsion and nanoparticles. The results revealed that the penetration of OMC into SC from the nanoparticulate formulation was 3.4-fold greater than that from an emulsion. This difference in the areas under the curves in Fig. 1 was highly significant (Student's *t* test, $p < 0.05$).

Though it is true that the level of surfactant in the NP appears to be rather high, this concentration is the same as that found in the conventional emulsion. The tape stripping results demonstrate clearly i) that this level of surfactant does not induce a catastrophic derangement of SC barrier function, and ii) that the better performance of the NP cannot simply be attributed to a skin penetration-enhancement effect of the surfactant alone.

This result was in agreement with previous studies, which reported that the use of particulate drug carriers (microparticles and nanoparticles) appeared to improve the drug residence in the skin without increasing transdermal transport. For example, Jenning *et al.* (6) demonstrated that vitamin A loaded solid lipid nanoparticles effectively delivered the vitamin to the upper skin layers, but did not appear to increase

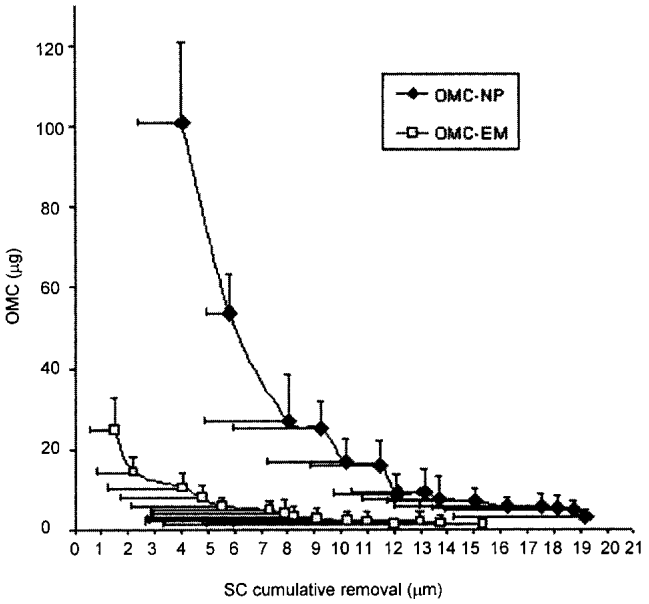

Fig. 1. Concentration profiles of OMC in porcine SC following delivery from an emulsion (OMC-EM) and from nanoparticles (OMC-NP) following a 6-h applications (n = 5; mean ± SD).

vitamin concentrations in the deeper skin strata. In addition, De Jalon *et al.* (7) reported that although PLGA-fluorescent microparticles were clearly visualized in the stratum corneum, epidermis and dermis, they were not able to reach the receptor compartment of the diffusion cells, even after a period of 24 h. The localization and quantification of particulate drug carriers are, therefore, of substantial interest in furthering our understanding of their mechanism of action.

A number of studies employing different techniques including diffusion experiments (16–23) visualization studies with electron microscopy (1), light microscopy (6,24), and fluoromicrography (7,25) have been conducted to investigate skin-particulate drug carrier interactions. A disadvantage of these microscopic techniques is that the tissue needs to be cryofixed, which may either change skin lipid organization or may result in redistribution of the label (26).

In order to visualize the nanoparticles in the skin, we chose to use confocal laser scanning microscopy (CLSM), since it allows the tissue to be optically sectioned and the distribution of the fluorescent probe in the sample to be observed in images parallel to the surface of the sample, without the need for tissue fixation.

However, because OMC is not fluorescent (and thus cannot be visualized by CLSM) a substitute model molecule, with similar physicochemical properties, was sought for encapsulation in the nanoparticles. We chose to load the P(CL) nanoparticles with Nile red, a powerful and highly lipophilic staining agent that been used for visualizing the intracellular lipids in the skin (27) . Like OMC, the high log $K_{o/w}$ of NR (~4) (28), ensures a high encapsulation efficiency in NP. Table I presents the physical parameters of the fluorescent formulation that was developed to perform the CLSM experiments. In the case of the Nile red nanoparticles (NR-NP), the high NR-encapsulation efficiency ensures that the fluorescence signal is sufficiently strong to allow detection by confocal microscopy.

The NR-nanoparticles were further characterized by investigating the *in vitro* release of NR from this system into IPM (Fig. 2). IPM was selected as a "receptor medium" which mimics the lipidic nature of the stratum corneum (SC) (29). A NR-propylene glycol solution (NR-PG) at the same Nile red concentration as the NR-nanoparticles was used as the control. As shown in Fig. 2, Nile red release from nanoparticles was greater than that from the PG solution. This difference in the extent of release of NR is probably due to a combination of various related factors. Because the Nile red–containing nanoparticles are surrounded by an aqueous milieu, the release of Nile red from the nanoparticles is influenced by the partitioning of the dye between the polymer-water and water-isopropyl myristate interfaces. However, the presence of nanoparticles at the aqueous:IPM interface enables the Nile red to be in close proximity to the IPM phase and circumvents the need for the dye to first partition into and then diffuse through an aqueous phase; furthermore, previous studies have shown that the NP polymer coat does not impede the release process: P(CL) is highly permeable to low molecular weight molecules (<400 Da) such as Nile red (MW = 318). Hence, once the NR-nanoparticles are in contact with the IPM phase, transfer of the dye from the interior of the nanoparticle into the IPM should be relatively rapid (30). Moreover, differences in thermodynamic activity due to different degrees of saturation of the dye in each formulation may also play an important role—an individual nanoparticle could be considered as a saturated system, that is, the maximum quantity of NR was encapsulated during nanoparticle preparation in contrast to NR-PG, which was not saturated—hence, the superior thermodynamic activity of the NR in the nanoparticles is expected to increase partitioning. Further, a saturated solution of the dye in PG (NR-S) was also tested in subsequent CLSM studies.

In the CLSM study, we microscopically observed the skin after the *in vitro* permeation of NR-NP and the two NR-control solutions: NR-PG and NR-S. The skin surface was defined as the imaging plane of brightest autofluorescence with a morphology characteristic of the SC surface. In the images of the SC surface (Fig. 3a, *xy*-direction,), the corneocyte groups form distinct "island-like" structures, separated by lipids that appear as dark furrows. Within the "island group," the corneocytes appear as polygonal shapes with a size of 10–30 µm, which corresponds to values reported in the

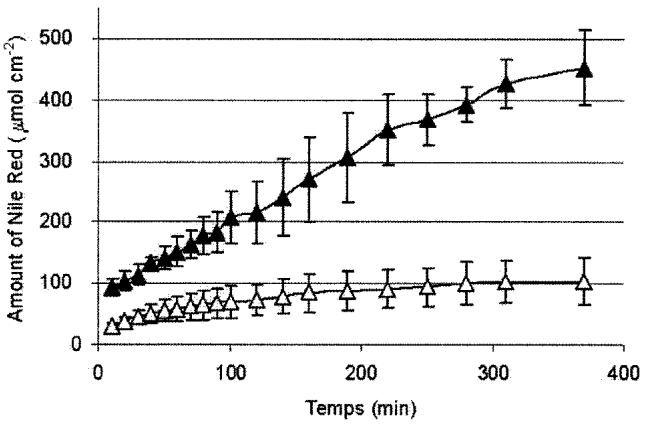

Fig. 2. Cumulative amounts of Nile red released from nanoparticles (▲) and from propylene glycol (△) as a function of time (mean ± SD, n = 8).

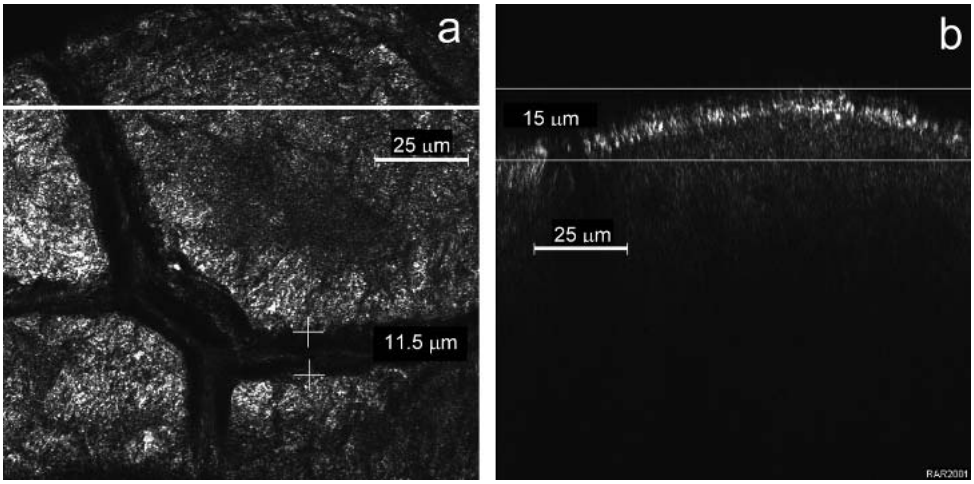

Fig. 3. CLSM images of porcine skin in the plane of the stratum corneum. (a) *xy*-direction, corneocytes are visualized due to the high auto-fluorescence of the tissue. The horizontal white line represents the position along which the *xz*-image in (b) was generated.

literature (31,32). Figure 3b is an optical image of the skin in the *xz*-direction.

The contribution of skin autofluorescence to the total fluorescence detected was corrected with the black level setting. Images of the skin pretreated with blank P(CL) nanoparticles did not reveal any fluorescence signal (results not shown). Figures 4, 5, and 6 consist of four representative, optical cross-sections, selected from several images and several different zones obtained in the *xz*-mode, of skin after application of NR-preparations for 0.5, 1, and 2 h, respectively. The fluorescence after NR-PG, NR-NP, and NR-S application can be observed in the lefthand, center and right-hand images, respectively.

The fluorescence distribution across the SC observed after treatment with NR-PG and NR-S is relatively homogeneous, as one might expect for a molecule that is extremely lipophilic. The images after application of the NR-formulations for 30 min are shown in Fig. 4 and there are no obvious differences in the fluorescence intensity observed after 30 min of NR permeation from each formulation. After a 1-h application of NR-NP (Fig. 5), an increased fluorescence intensity was observed; furthermore, the fluorescence also

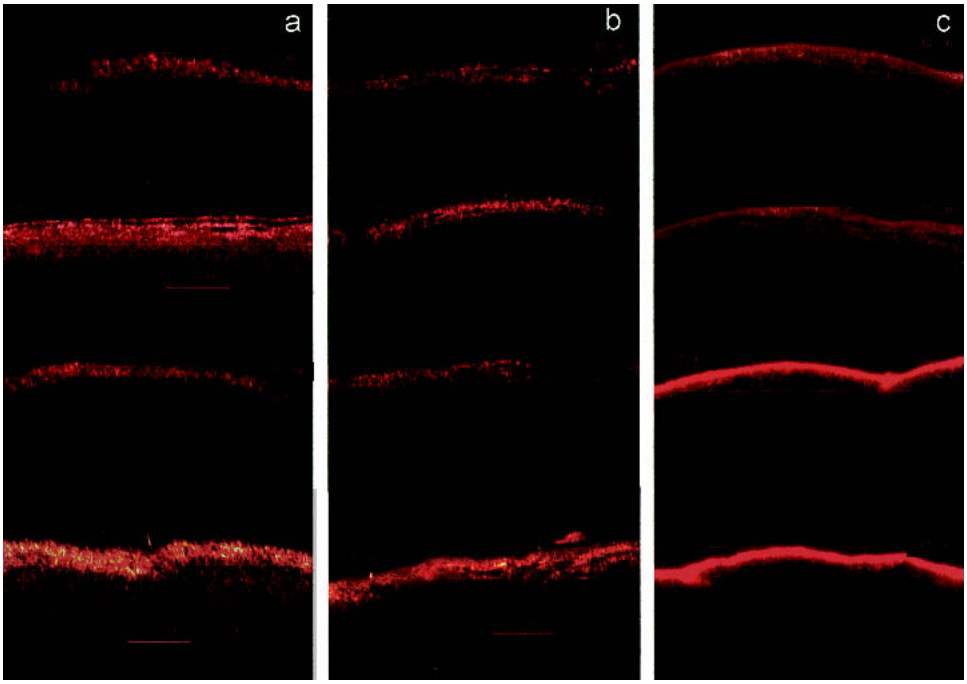

Fig. 4. Cross-sectional images obtained following 30 min of passive permeation. (a) Nile red solution in propylene glycol at the same concentration as Nile red in nanoparticles (NR-PG); (b) Nile red nanoparticles (NR-NP) and (c) Nile red saturated solution in propylene glycol (NR-S). Note that in this figure, the fluorescence distribution from the three formulations is not different.

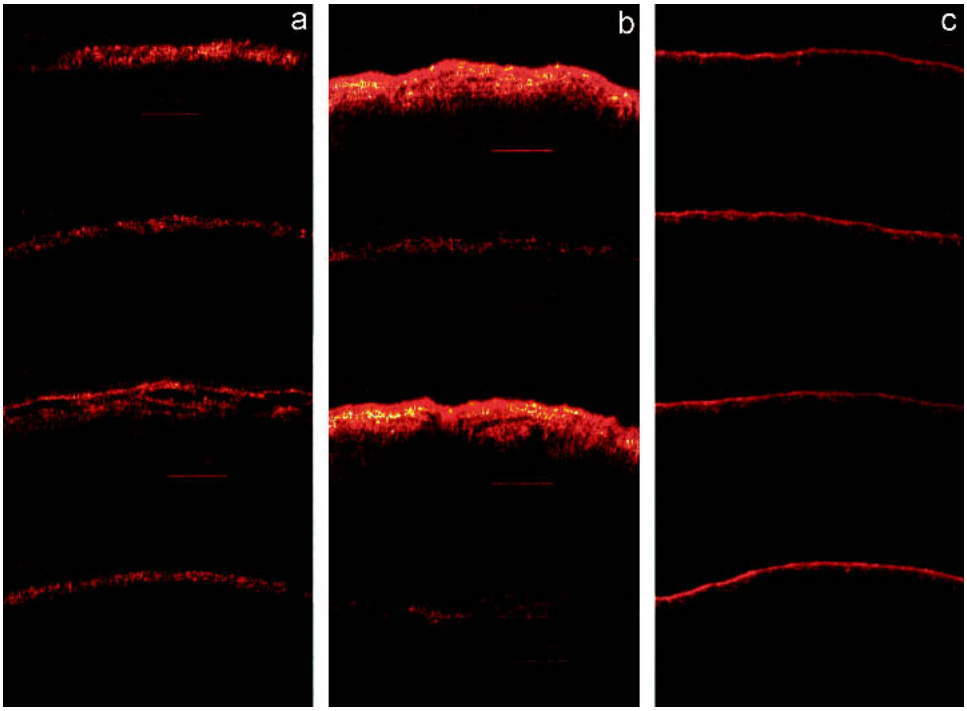

Fig. 5. Cross-sectional images obtained following 1 h of passive permeation. (a) Nile red solution in propylene glycol at the same concentration as Nile red in nanoparticles (NR-PG); (b) Nile red nanoparticles (NR-NP) and (c) Nile red saturated solution in propylene glycol (NR-S). The fluorescence intensity subsequent to treatment with the NR-NP formulation is higher and present to a greater skin depth compared to the other formulations.

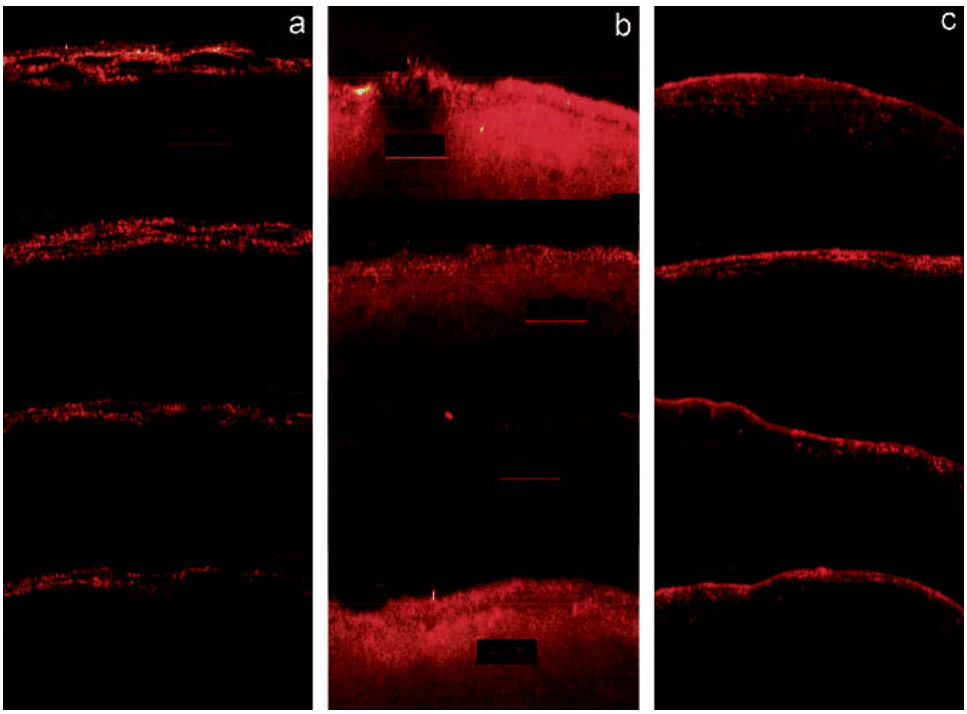

Fig. 6. Cross-sectional images obtained following 2 h of passive permeation. (a) Nile red solution in propylene glycol at the same concentration as Nile red in nanoparticles (NR-PG); (b) Nile red nanoparticles (NR-NP) and (c) Nile red saturated solution in propylene glycol (NR-S). Note that in this figure, the fluorescence distribution from the NR-NP was much more marked with fluorescence perceptible down to 60 μm.

persisted to a greater depth in the skin. In the NR-PG and NR-S images, the fluorescence intensity diminishes rapidly with depth. After 2 h (Fig. 6), the increased distribution and much greater permeation from the NR-NP was marked, with fluorescence perceptible down to 60 μm.

The increased fluorescence intensity and greater extent of penetration observed following NR-NP application is in agreement with the release data presented in Fig. 2, which show significantly higher dye release from the nanoparticles. Other phenomena present in the skin, may also increase the partitioning and penetration of Nile red from the nanoparticles in the membrane. It is conceivable that the furrows between the corneocyte islands provide a place into which the nanoparticles may accumulate within the skin. Therefore, in the case of a highly lipophilic molecule, the nanoparticles (e.g., NR-NP) facilitate transport of the molecule to deeper layers in the skin from where the molecule is released into the lipid matrix and can diffuse further into the tissue. Additional studies are obviously needed to test these hypotheses.

CONCLUSIONS

The encapsulation of a highly lipophilic molecule (OMC) using polymeric nanoparticles significantly enhanced the penetration of the molecule into the stratum corneum layers, compared to a non-particulate formulation at the same concentration, without detectable permeation into the receiver phase. To probe further the mechanism of this enhancement, a surrogate lipophilic molecule (Nile red) was encapsulated in an identical nanoparticulate system. By virtue of its fluorescence, the cutaneous distribution of NR delivered from various formulations could be visualized using CLSM. The confocal images clearly demonstrated the enhanced distribution of NR (greater quantities of NR delivered to deeper regions) when delivered from P(CL) nanoparticles. These studies did not permit us to determine unequivocally whether the fluorescence observed in the CLSM images originated from NR associated with the nanoparticle or from free NR (released from the nanoparticle) and this is the subject of further investigation in our laboratory. It is plausible that skin structures provide channels that enable the nanoparticles to access deeper tissue layers from where the permeant is gradually released by passive diffusion into the neighboring environment. As a result of the relatively uniform and intense distribution of NR fluorescence, it was not possible to identify specific skin structures, for example, hair follicles, which might have served as shunt pathways for transport across the skin. The molecules contained in the nanoparticles may also be at higher thermodynamic activity relative to solution formulations, which would also facilitate their partitioning into the membrane. The physical effect of a high specific surface area of the nanoparticles may also play an important role in dermal penetration. This high specific surface area of nanometer-sized particles facilitates contact of encapsulated molecule with the stratum corneum. Such a system offers the potential for targeted delivery to the skin surface—as may be desired for substrates such as sunscreen agents.

ACKNOWLEDGMENTS

Rocío Alvarez Román is the recipient of a grant from CONACyT-SFERE, México-France.

REFERENCES

1. A. Rolland, N. Wagner, A. Chatelus, B. Shroot, and H. Schaefer. Site-specific drug delivery to pilosebaceous structures using polymeric microspheres. *Pharm. Res.* **10**:1738–1744 (1993).
2. E. G. de Jalon, M. J. Blanco-Prieto, P. Ygartua, and S. Santoyo. Topical application of acyclovir-loaded microparticles: quantification of the drug in porcine skin layers. *J. Control. Rel.* **75**:191–197 (2001).
3. S. A. Wissing and R. H. Muller. Solid lipid nanoparticles as carrier for sunscreens: *in vitro* release and *in vivo* skin penetration. *J. Control. Rel.* **81**:225–233 (2002).
4. A. Dingler, R. P. Blum, H. Niehus, R. H. Muller, and S. Gohla. Solid lipid nanoparticles (SLN/Lipopearls)–a pharmaceutical and cosmetic carrier for the application of vitamin E in dermal products. *J. Microencapsul.* **16**:751–767 (1999).
5. V. Jenning, M. Schafer-Korting, and S. Gohla. Vitamin A-loaded solid lipid nanoparticles for topical use: drug release properties. *J. Control. Rel.* **66**:115–126 (2000).
6. V. Jenning, A. Gysler, M. Schafer-Korting, and S. H. Gohla. Vitamin A loaded solid lipid nanoparticles for topical use: occlusive properties and drug targeting to the upper skin. *Eur. J. Pharm. Biopharm.* **49**:211–218 (2000).
7. E. G. de Jalon, M. J. Blanco-Prieto, P. Ygartua, and S. Santoyo. PLGA microparticles: possible vehicles for topical drug delivery. *Int. J. Pharm.* **226**:181–184 (2001).
8. J.-P. Devissaguet, H. Fessi, and F. Puisieux. Process for the preparation of dispersable colloidal systems of substance in the form of nanocapsules. U.S. patent 5,049,322.
9. S. S. Guterres, H. Fessi, G. Barratt, J.-P. Devissaguet, and F. Puisieux. Poly(-lactide) nanocapsules containing diclofenac: I. Formulation and stability study. *Int. J. Pharm.* **113**:57–63 (1995).
10. G. Potard, C. Laugel, A. Baillet, H. Schaefer, and J. P. Marty. Quantitative HPLC analysis of sunscreens and caffeine during *in vitro* percutaneous penetration studies. *Int. J. Pharm.* **189**:249–260 (1999).
11. P. Calvo, J. L. Vila-Jato, and M. J. Alonso. Comparative in vitro evaluation of several colloidal systems, nanoparticles, nanocapsules, and nanoemulsions, as ocular drug carriers. *J. Pharm. Sci.* **85**:530–536 (1996).
12. V. Ferranti, H. Marchais, C. Chabenat, A. M. Orecchioni, and O. Lafont. Primidone-loaded poly-varε-caprolactone nanocapsules: incorporation efficiency and *in vitro* release profiles. *Int. J. Pharm.* **193**:107–111 (1999).
13. R. Alvarez-Román, G. Barré, R. H. Guy, and H. Fessi. Biodegradable polymer nanocapsules containing a sunscreen agent: preparation and photoprotection. *Eur. J. Pharm. Biopharm.* **52**: 191–195 (2001).
14. F. Benech-Kieffer, P. Wegrich, R. Schwarzenbach, G. Klecak, T. Weber, J. Leclaire, and H. Schaefer. Percutaneous absorption of sunscreens *in vitro*: interspecies comparison, skin models and reproducibility aspects. *Skin Pharmacol. Appl. Skin Physiol.* **13**: 324–335 (2000).
15. M. B. Reddy, A. L. Stinchcomb, R. H. Guy, and A. L. Bunge. Determining dermal absorption parameters *in vivo* from tape strip data. *Pharm. Res.* **19**:292–298 (2002).
16. N. Katahira, T. Murakami, S. Kugai, N. Yata, and M. Takano. Enhancement of topical delivery of a lipophilic drug from charged multilamellar liposomes. *J. Drug Target.* **6**:405–414 (1999).
17. M. K. Kim, S. J. Chung, M. H. Lee, A. R. Cho, and C. K. Shim. Targeted and sustained delivery of hydrocortisone to normal and stratum corneum-removed skin without enhanced skin absoption using a liposome gel. *J. Controlled Release* **46**:243–251 (1997).
18. Y. Hsiu-Ying and L. Hui-Min. Triamcinolone permeation from different liposome formulations through rat skin *in vitro*. *Int. J. Pharm.* **127**:1–7 (1996).
19. J. du Plessis, C. Ramachandran, N. Weiner, and D. G. Muller. The influence of particle size of liposomes on the deposition of drug into skin. *Int. J. Pharm.* **103**:277–282 (1994).
20. G. M. El Maghraby, A. C. Williams, and B. W. Barry. Skin delivery of oestradiol from lipid vesicles: importance of liposome structure. *Int. J. Pharm.* **204**:159–169 (2000).
21. G. M. El Maghraby, A. C. Williams, and B. W. Barry. Oestradiol

skin delivery from ultradeformable liposomes: refinement of surfactant concentration. *Int. J. Pharm.* **196**:63–74 (2000).
22. E. Touitou, N. Shaco-Ezra, N. Dayan, M. Jushynski, R. Rafaeloff, and R. Azoury. Dyphylline liposomes for delivery to the skin. *J. Pharm. Sci.* **81**:131–134 (1992).
23. K. Egbaria, C. Ramachandran, and N. Weiner. Topical application of liposomally entrapped cyclosporin evaluated by *in vitro* diffusion studies with human skin. *Skin Pharmacol.* **4**:21–28 (1991).
24. S. M. Niemiec, J. M. Latta, C. Ramachandran, N. D. Weiner, and B. J. Roessler. Perifollicular transgenic expression of human interleukin-1 receptor antagonist protein following topical application of novel liposome- plasmid DNA formulations in vivo. *J. Pharm. Sci.* **86**:701–708 (1997).
25. J. Lasch, R. Laub, and W. Wohlrab. How deep intact liposomes penetrate into human skin? *J. Control. Rel.* **18**:55–58 (1991).
26. D. M. Shotton. Confocal scanning optical microscopy and its applications for biological specimens. *J. Cell Sci.* **94**:175–206 (1989).
27. A. Entwistle and M. Noble. The quantification of fluorescent emission from biological samples using analysis of polarization. *J. Microsc.* **165**:347–365 (1992).
28. N. G. Turner and R. H. Guy. Iontophoretic transport pathways: dependence on penetrant physicochemical properties. *J. Pharm. Sci.* **86**:1385–1389 (1997).
29. B. W. Barry. Basic principles of diffusion through membranes. In J. Swarbrick (ed.), *Dermatological Formulations. Percutaneous Absorption*, Marcel Dekker, New York, 1983, pp. 49–94.
30. P. Greenspan, E. P. Mayer, and S. D. Fowler. Nile red: a selective fluorescent stain for intracellular lipid droplets. *J. Cell Biol.* **100**: 965–973 (1985).
31. M. E. Meuwissen, J. Janssen, C. Cullander, H. E. Junginger, and J. A. Bouwstra. A cross-section device to improve visualization of fluorescent probe penetration into the skin by confocal laser scanning microscopy. *Pharm. Res.* **15**:352–356 (1998).
32. M. Rajadhyaksha, S. Gonzalez, J. M. Zavislan, R. R. Anderson, and R. H. Webb. I*n vivo* confocal scanning laser microscopy of human skin II: advances in instrumentation and comparison with histology. *J. Invest. Dermatol.* **113**:293–303 (1999).